Dynamics of microdroplet generation via drop impact on a superhydrophobic micropore ⊕ ✓

Mohammad Shibli Reza (محمد شبلی رضا); Young-Su Ko (고영수); Byeong Eun Jeon (전병은); Prosenjit Sen (প্রসেনজিৎ সেন); Choongyeop Lee (이충엽) ✉ ⓘD

Check for updates

View Online

Export Citation

Physics of Fluids

Special Topic:
Recent Advances in Fluid Dynamics and its Applications

Guest Editors: B.Reddappa, B. Rushi Kumar, Sreedhara Rao Gunakala, Bijula Prabhakar Reddy

Submit Today!

AIP Publishing

AIP Publishing

Dynamics of microdroplet generation via drop impact on a superhydrophobic micropore (EP)

Mohammad Shibli Reza (محمد شبلی رضا),[1] Young-Su Ko (고영수),[1] Byeong Eun Jeon (전병은),[1]
Prosenjit Sen (প্রসেনজিৎ সেন),[2] and Choongyeop Lee (이충엽)[1,a] (iD)

AFFILIATIONS

[1]Department of Mechanical Engineering (Integrated Engineering Program), Kyung Hee University, Yongin-si 17104,
Republic of Korea
[2]Centre for Nano Science and Engineering, Indian Institute of Science, Bangalore 560012, India

[a]Author to whom correspondence should be addressed: cylee@khu.ac.kr

ABSTRACT

This study delves into the dynamics of generating microdroplets by impacting a droplet onto a micropore on superhydrophobic copper substrates. It identifies the necessary impact velocities for single microdroplet formation for each micropore and characterizes microdroplet size in relation to micropore diameter. The results underscore the significant role of viscosity, especially as the diameter of the micropore decreases. For micropores measuring $400\,\mu m$, an increase in viscosity up to 8 cP does not alter the critical impact velocities, while smaller diameters of 50 and $100\,\mu m$ see a notable change in critical velocities with even minor increases in viscosity. Remarkably, the diameter of the microdroplet remains consistent regardless of changes in the liquid viscosity or impact velocity. This research showcases two practical uses of single microdroplets: printing on paper and fabricating microbeads. The insights gained from these findings pave the way for advancements in printing technology and microfabrication techniques.

Published under an exclusive license by AIP Publishing. https://doi.org/10.1063/5.0207480

I. INTRODUCTION

Over the years, researchers have extensively investigated the dynamics of drop impact on solid surfaces due to its diverse applications in biomedical diagnostics,[1] food processing[2] and chemical industries,[3] electronic industries,[4] and rapid prototyping.[5,6] Notably, it has been demonstrated that drop impact on a mesh with micropores can serve as a mechanism to generate microdroplets.[7] This technique requires a superhydrophobic mesh and precise control of impact velocity to effectively produce microdroplets. These microdroplets, comprising various liquids, hold potential applications in semiconductor technology, thermal management, biotechnology, and 3D printing.[8,9] The innovative approach to microdroplet generation through drop impact offers distinct advantages over conventional printing techniques, as traditional methods often face critical issues such as nozzle clogging,[10] leading to increased maintenance costs and design complexities.[11]

Recently, with advancements in surface modification techniques, the study of drop impact on solid surfaces concerning specific surface wettability (e.g., hydrophobicity[12,13] and hydrophilicity[14,15]), which is determined by the surface energy and surface roughness,[16] has gained attention. Wettability is commonly assessed in terms of the contact angle of a water drop on the surface. Surfaces with contact angles below 90° are considered hydrophilic, indicating a strong affinity toward water, while those with contact angles above 90° are regarded as hydrophobic, displaying strong water repellency. Contact angles above 150° require additional surface structures to amplify hydrophobicity, a property termed superhydrophobic (SHPo).[17,18] These SHPo surfaces are found among many plants and insects in nature.[19,20]

The SHPo property results from reduced water–solid contact when a water drop is deposited on the surface. The water only touches the top of surface structures, leading to diminished water adhesion and increased contact angle.[21,22] Due to a remarkably high water drop mobility on SHPo surfaces, SHPo surfaces have earned considerable attention, prompting the implementation of various techniques to create these ultra-repellent surfaces by combining tailored surface roughness with hydrophobic coatings.[23–26] Their exceptional water mobility and minimal viscous dissipation make SHPo surfaces well suited for exploring novel drop dynamics.[27,28]

In particular, drop impact studies on porous mesh surfaces have gained popularity due to their widespread applications in various industries.[9,29,30] Understanding drop dynamics at a single pore level can elucidate water penetration mechanism on multipored structures

07 June 2024 05:18:57

or meshes. During drop impact on a typical SHPo surface, the drop kinetic energy is transferred to surface energy with minimal viscous dissipation, while the drop undergoes spreading and retracting. Meanwhile, on surfaces with pores, the dynamic pressure associated with impact velocity U_0 competes with the opposing effect of capillary pressure manifested by the meniscus formed inside the pore.[29,31] When the dynamic pressure is larger than the capillary pressure inside the pore, two scenarios can be envisaged. When the dynamic pressure is sufficiently high, the liquid jet is formed through the pore and breaks up into smaller droplets due to Rayleigh–Plateau instability.[32,33] On the other hand, at a lower dynamic pressure, these liquid jets might return back to the pore surface without fragmentation.

It is worth noting that several studies on liquid penetration have been conducted considering various factors, such as surface wettability, impact velocity, and liquid properties.[34–36] However, these works focus on mesh having multiple pores, which is not an ideal platform to study drop penetration dynamics on a single pore level. Moreover, previous studies investigating single pores were restricted to observing water penetration through hydrophilic pores rather than superhydrophobic (SHPo) pores.[29,37] In this study, we focus on drop impact on a single SHPo micrometer-sized pore as well as subsequent microdroplet generation. Note that the SHPo surface is crucial to ensure complete separation of the micro-droplet from the pore. Our main objectives are to study single microdroplet generation at a micrometer scale via drop impact on a single micropore, understand post-generation dynamics of microdroplets, and demonstrate potential applications including microdroplet printing and microbead formation. Additionally, our study demonstrates the possibility of generating a single micro-droplet with viscous liquids, establishing the suitability of this technique for a wider range of liquids beyond water.

II. EXPERIMENTAL SETUP AND TECHNIQUES
A. Fabrication of pore surfaces

For this study, 1 mm thick commercial copper plates were used as the substrate. Initially micropores of four different sizes were created through micro-drilling, as shown in Fig. 1(a). These micropores were designated with diameters of 50, 100, 200, and 400 μm.

Following the creation of micropores, the copper plates were cleaned with acetone, ethanol, and de-ionized (DI) water. Subsequently, copper (Cu) plates were dipped in a 3M HCl aqueous solution to remove the native oxide from the copper surface. Then, an aqueous solution comprising 5 g NaOH, 10 g Na$_3$PO$_4$, 3.75 g NaClO$_2$ in 100 ml DI water was prepared. The Cu plates were then immersed in the heated aqueous solution (at 85 °C) for 30 min to form a uniform oxide nanostructure on the plates.[38] Following this step, the Cu samples were coated with a hydrophobic self-assembly monolayer using a vapor deposition method involving HDFS (1H, 1H, 2H, 2H-perfluorodecyltrimethoxysilane, Sigma-Aldrich) and toluene in a volume ratio of 1:9. Through this process, the SHPo surface property was obtained within a single micropore. The prepared SHPo surfaces were examined using Scanning Electron Microscopy (SEM). Insets of Fig. 1(a) display the magnified images of the 200 μm pore surface. The static contact angle of water drops on the SPHo surfaces was found to range between 165° and 175° [Fig. 1(c)].
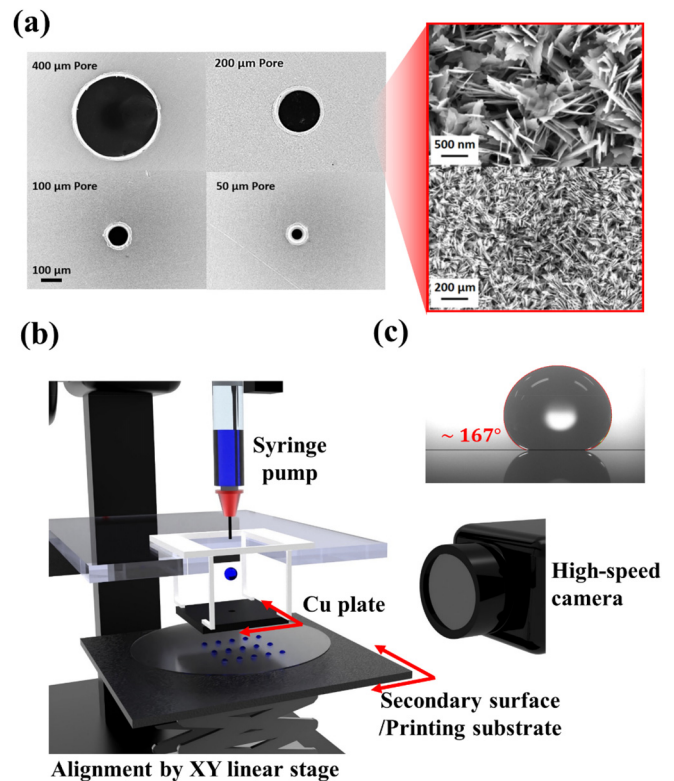

FIG. 1. (a) SEM images of a single pore on superhydrophobic surfaces. (b) Schematic of experimental setup. (c) Contact angle of the water droplet on CuO superhydrophobic substrate.

B. Experimental details

The experimental setup is shown in Fig. 1(b). A syringe pump (UMP3 Ultra micropump) was used to generate controlled water drops through the attached syringe tip (Nordson-PN:7018462) with an outer diameter of 0.24 mm, resulting in drops 2.3 mm in diameter. To ensure controlled drop impact at the center of the micropore, the substrate was mounted on a movable linear stage, and its position was adjusted before each trial. When necessary, another SHPo surface was positioned beneath the surface with a single micropore to analyze the dynamics of the generated microdroplets. The impact velocity was varied between 0.5 and 2.0 m/s by adjusting the height of the syringe tip releasing the water drop. It was found that SHPo coating within a micropore guarantees complete removal of liquid following each experimental trial.

Events following drop impact on a single micropore were captured using a high-speed camera (Phantom VE0410L) equipped with a Nikon 36X zoom lens positioned at the same horizontal plane as the substrate with a micropore. Additionally, a high-intensity LED source was placed at the opposite end of the camera for proper illumination. Recordings were made at up to 50 000 frames per second with an exposure time of 20 μs. Synchronization between drop release from the syringe tip and recording was achieved using a computer connected to a camera. The entire sequence, including drop impact on the pore surface, penetration dynamics through the pore, and generation

of microdroplet after penetration, were recorded. After each experiment, any residual liquid was removed, and the surface was ensured to be dry before conducting a new experiment. All experiments were conducted at a controlled room temperature of 22.5–23.1 °C.

III. RESULTS AND DISCUSSION

A. Microdroplet generation

Figure 2(a) presents a time sequence of images illustrating the microdroplet generation during drop impact on a 400 μm micropore, while Fig. 2(b) is the schematic of the microdroplet generation. At 1 ms after impact, penetration through a micropore is observed to occur. Then, at 2 ms after impact, a microdroplet is separated from a parent drop, resulting in a successful generation of a single microdroplet. The mechanism of microdroplet generation can be understood by the balance between inertial force and surface tension within a micropore. As the drop hits the micropore, it applies a dynamic pressure while surface tension acts upward to keep the liquid from penetrating. As shown in Fig. 2(c), to get a successful penetration, this inertial force ($\rho U_0^2 d_p^2$) must overcome the capillary force (γd_p), yielding the penetration criterion, $U_0 > C\sqrt{\gamma/\rho d_p}$, where U_0 is the impact velocity, γ is the surface tension, C is the numerical coefficient on the order of unity, ρ is the density of the liquid, and d_p is the pore diameter.[9]

Figure 3(a) shows how the impact velocity U_0 affects microdroplet generation through a micropore 200 μm in diameter (microdroplet generation through 100 μm is shown in Fig. S1). If the impact velocity U_0 is sufficiently large, a water drop completes the penetration and generates microdroplets (as in the case of $U_0 = 1.17$, 1.52, and 1.91 m/s). However, at a smaller U_0, the generation of microdroplet does not occur, even if the water penetrates through a micropore (as in the case of $U_0 = 1.04$ m/s).

Figure 3(b) shows more details about the microdroplet generation as a function of micropore diameter. The dashed line shows the theoretical criterion for liquid penetration through a micropore.[9] Here, U_{cr} is the minimum impact velocity for successful liquid penetration, and it is comparable to $U_{cr} \sim \sqrt{\gamma/\rho d_p}$, which agrees with the experimental

observation that a larger pore diameter (d_p) results in a lower critical impact velocity (U_{cr}).

As observed in Fig. 3(a), the occurrence of liquid penetration is not sufficient to generate microdroplets and an impact velocity much higher than the critical velocity for penetration [U_{cr}, a dotted line in Fig. 3(b)] is required for microdroplet generation. At U_{cr}, the inertial force ($\rho U_{cr}^2 d_p^2$) is comparable to the capillary force (γd_p), and on further increase in the impact velocities an inertial force prevails and ensures the formation of a longer jet with length l, which breaks up into a single microdroplet or multiple microdroplets, as shown in Fig. 2(c). In Fig. 3(b), regimes for a microdroplet generation are defined: (i) The *no generation* regime is marked by no microdroplet generation through micropore. This regime includes "*no liquid penetration through a micropore*" and "*liquid penetration through a micropore, but no separation of microdroplets*," where the dashed line in Fig. 3(b) marks the boundary between the two. The "no penetration" regime is identified by $U_o < 1.51$ m/s ($d_p = 50$ μm), 1.30 m/s ($d_p = 100$ μm), 1.07 m/s ($d_p = 200$ μm), and 0.85 m/s ($d_p = 400$ μm). (ii) The *single microdroplet generation* regime is marked by successful generation of a single microdroplet through a micropore [shaded region in Fig. 3(b)]. The impact velocity shows a linear decrement with increase in the pore size. The impact velocities for this regime fall within the range $1.53 < U_o < 1.71$ m/s ($d_p = 50$ μm), $1.33 < U_o < 1.53$ m/s ($d_p = 100$ μm), $1.08 < U_o < 1.25$ m/s ($d_p = 200$ μm), and $0.88 < U_o < 1.04$ m/s ($d_p = 400$ μm). (iii) The *double and multiple microdroplet generation* regime is characterized by the formation of a sufficiently longer jet followed by the generation of multiple microdroplets as a result of a breaking up of a jet. The ejected liquid jet breaks up into multiple microdroplets due to Rayleigh–Plateau instability, and these microdroplets traverse the air until they reach the substrate. They maintain similar velocities, preventing recombination during flight.

Here, we focus on a single microdroplet generation from a micropore with different diameters. After the regime for a single microdroplet generation was determined, the diameter of the generated
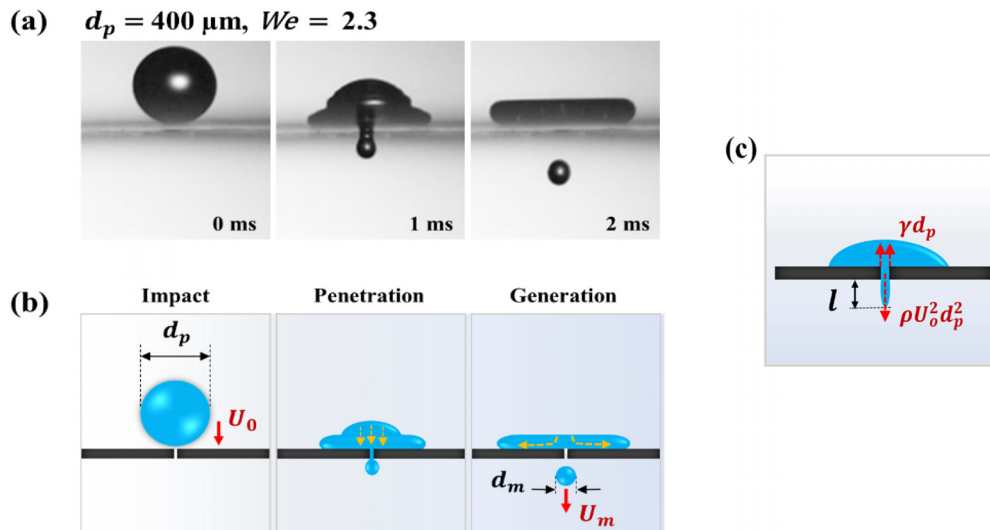
FIG. 2. (a) Drop impact dynamics on micropore surface with 400 μm diameter. (b) Schematic of drop impact dynamics on a single micropore. (c) Schematic showing parameters influencing a microdroplet generation.
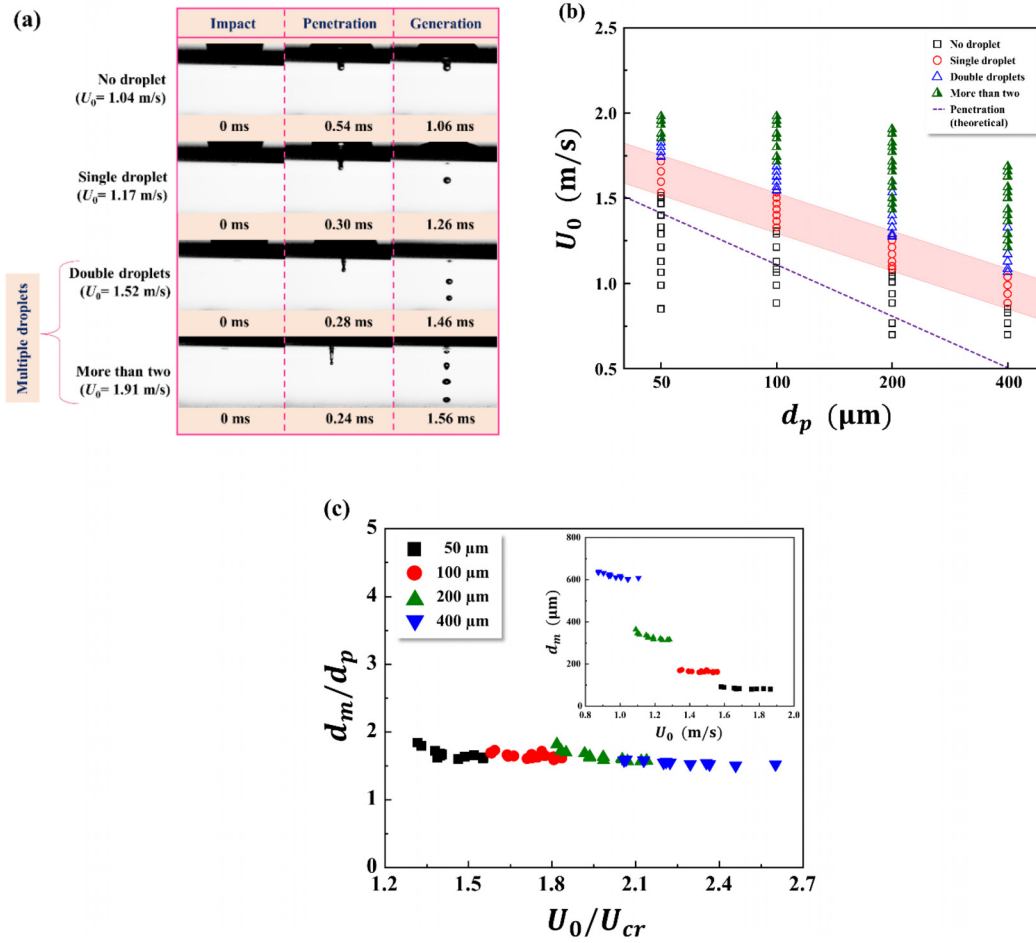
FIG. 3. (a) Time sequence images of microdroplet generation through 200 μm pore depending on the impact velocity U_0. (b) Regimes of microdroplet generation as a function of the impact dynamics U_0 for a micropore 50, 100, 200, and 400 μm in diameter. (c) The normalized microdroplet diameter as a function of the normalized impact velocity.

microdroplet was measured. According to the Rayleigh–Plateau instability, the volumes of the separated jet and microdroplet should be identical, that is, $\pi(d_p/2)^2 l \cong 4\pi/3\,(d_m/2)^3$, where l represents the maximum jet length before separation and d_m represents the diameter of the generated microdroplet. Meanwhile, l can be assumed to be the wavelength corresponding to the fastest instability mode, such as $l/d_p \approx 4.5$, which yields $d_m/d_p \approx 1.89$. As depicted in the inset of Fig. 3(c), in the impact velocity U_0 corresponding to a single microdroplet generation, the microdroplet diameter increases with the micropore diameter, while it remains nearly constant with the change of U_0. When the microdroplet diameter is normalized with the micropore diameter, the measured d_m/d_p is in the range of $1.5-1.8$, close to the predicted value of 1.89.

In practical scenarios requiring continuous droplet ejection, the timing between collisions is crucial. For single microdroplet generation, we can adjust the interval between generations by controlling the drop impact frequency. The minimum interval is determined by the contact time of the drop with the SHPo substrate, typically around 10 ms for drops of millimeter size.[39] In contrast, when generating multiple droplets, the interval between collisions is dictated by both the velocity of the microdroplets and the spacing between them. For example, with a 200 μm micropore, the jet velocity is approximately 0.6 m/s [Fig. 5(b)], and the center-to-center distance is about 1 mm ($l/d_p \approx 4.5$ from Rayleigh–Plateau instability), resulting in an interval of roughly 1.7 ms. For a 50 μm micropore, a similar analysis indicates an interval of about 0.14 ms, illustrating that the time between collisions diminishes as the pore size decreases.

B. The influence of liquid viscosity on microdroplet generation

This section discusses how the liquid viscosity modifies microdroplet generation. The viscosity is varied to lie in the range 1–62 centipoise by varying the mixing ratio of glycerin in aqueous solution (see supplementary Table 1). Experiments have been conducted to define a range of impact velocities for a single microdroplet generation. Figures 4(a) and 4(b) display the required impact velocity for a single microdroplet generation through 400 and 200 μm pores, respectively, which
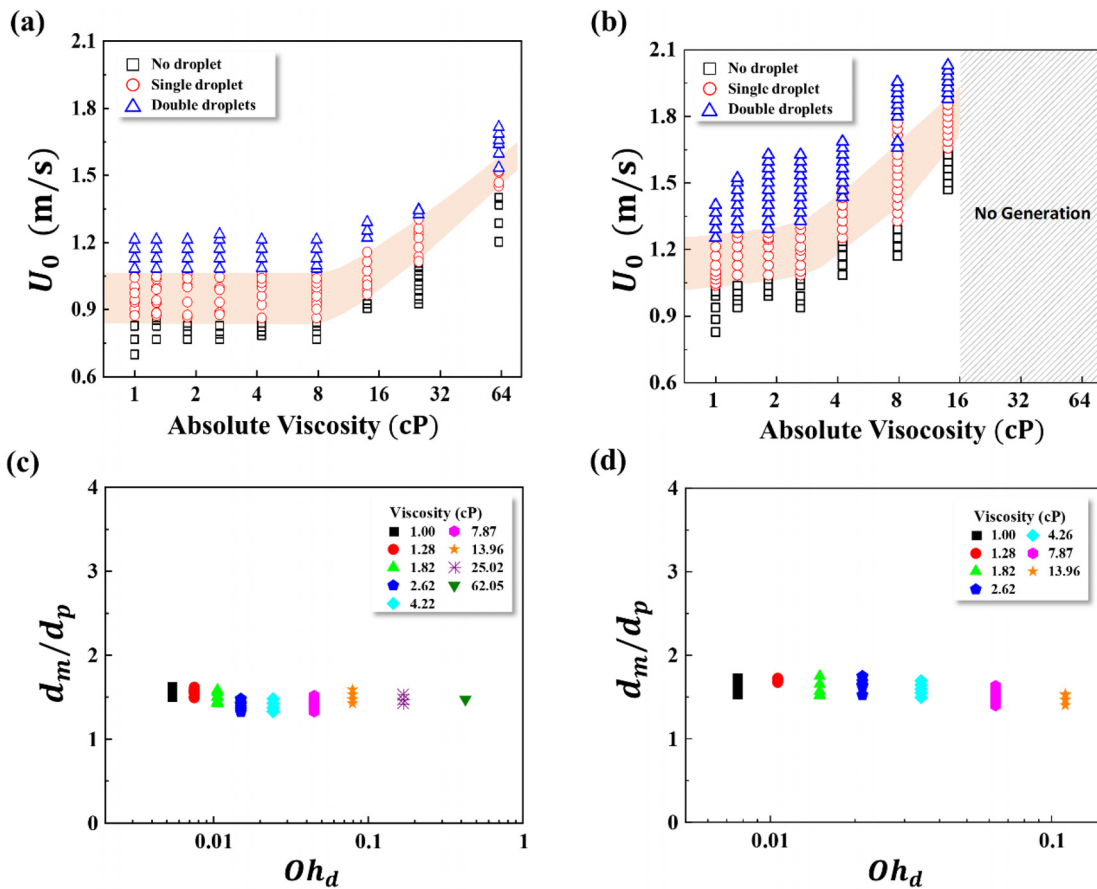
FIG. 4. Microdroplet generation through micropore of size (a) 400 μm and (b) 200 μm using a viscous liquid. (c) Drop size through a 400 μm pore as a function of the Ohnesorge number. (d) Drop size through a 200 μm pore as a function of the Ohnesorge number.

is highlighted with the shaded region. From the graphs, it is interesting to note that as the viscosity increases up to a certain value, the critical impact velocity for microdroplet generation does not change much. After that, it increases significantly. Quéré *et al.*[29] discussed the effect of viscous force on liquid penetration by considering the balance among the inertial force, the viscous force, and the capillary force, such that $\rho U_0^2 d_p^2 \sim \mu U_0 d_P + \gamma d_P$, where μ is the liquid viscosity. Although this equation was initially proposed to explain the liquid penetration, the basic dynamics applies equally to microdroplet generation, such that increase in the viscous force requires a larger inertial force, i.e., a higher impact velocity.

At a low viscosity (cP < 8, for 400 μm pore diameter and cP < 3 for 200 μm pore diameter), the viscous effect is not very pronounced. Neglecting the viscous force, the inertial force directly equates with the capillary force, resulting in $U_0 \sim \sqrt{\gamma/\rho d_P}$. With further increase in the liquid viscosity, the viscous factor becomes dominant over the capillary force, while the inertial force is comparable to the viscous force, that is, $U_0 \sim \mu/(\rho d_P)$. This explains the increase in critical impact velocity for microdroplet generation only beyond a certain viscosity value.

Moreover, the two relations can explain the increase in impact velocity with decreasing pore size. In a low viscosity regime, which is identified by cP < 8, for $d_p = 400$ μm and cP < 3 for $d_p = 200$ μm, the

capillary force (γd_P) is a primary opposing force against the inertial force with $U_0 \sim \sqrt{\gamma/\rho d_P}$. Meanwhile, at a higher viscosity (cP ≥ 8, for 400 μm and cP ≥ 3 for 200 μm pores), the balance between the inertial force and the viscous force leads to $U_0 \sim \mu/(\rho d_P)$ with different functional dependence on d_P. This difference explains the shrinkage of low viscosity regime with decreasing pore size, which is indeed experimentally observed. It also suggests that an increase in viscosity would have a more significant effect on the critical impact velocity for microdroplet generation in the case of smaller pores. Indeed, with even a slight increase in viscosity, microdroplet generation could not be obtained for $d_p \leq 100$ μm, as the required impact velocity for microdroplet generation is beyond the maximum allowable value in our experimental setup (see Fig. S2).

It is interesting to study how the liquid viscosity would affect the diameter of the generated microdroplets (d_m/d_p), where the viscosity effect is expressed using the Ohnesorge number, $Oh = \mu/\sqrt{\rho\gamma d_P}$. Figures 4(c) and 4(d) show that the normalized microdroplet diameter does not change appreciably with Oh, indicating that the microdroplet generation mechanism is rather insensitive to the liquid viscosity. Similar to the previous result where the working fluid was DI water [Fig. 3(c)], here also, the relative microdroplet diameter to the pore diameter (d_m/d_p) is found to be 1.5–1.8. Note that this result is in line
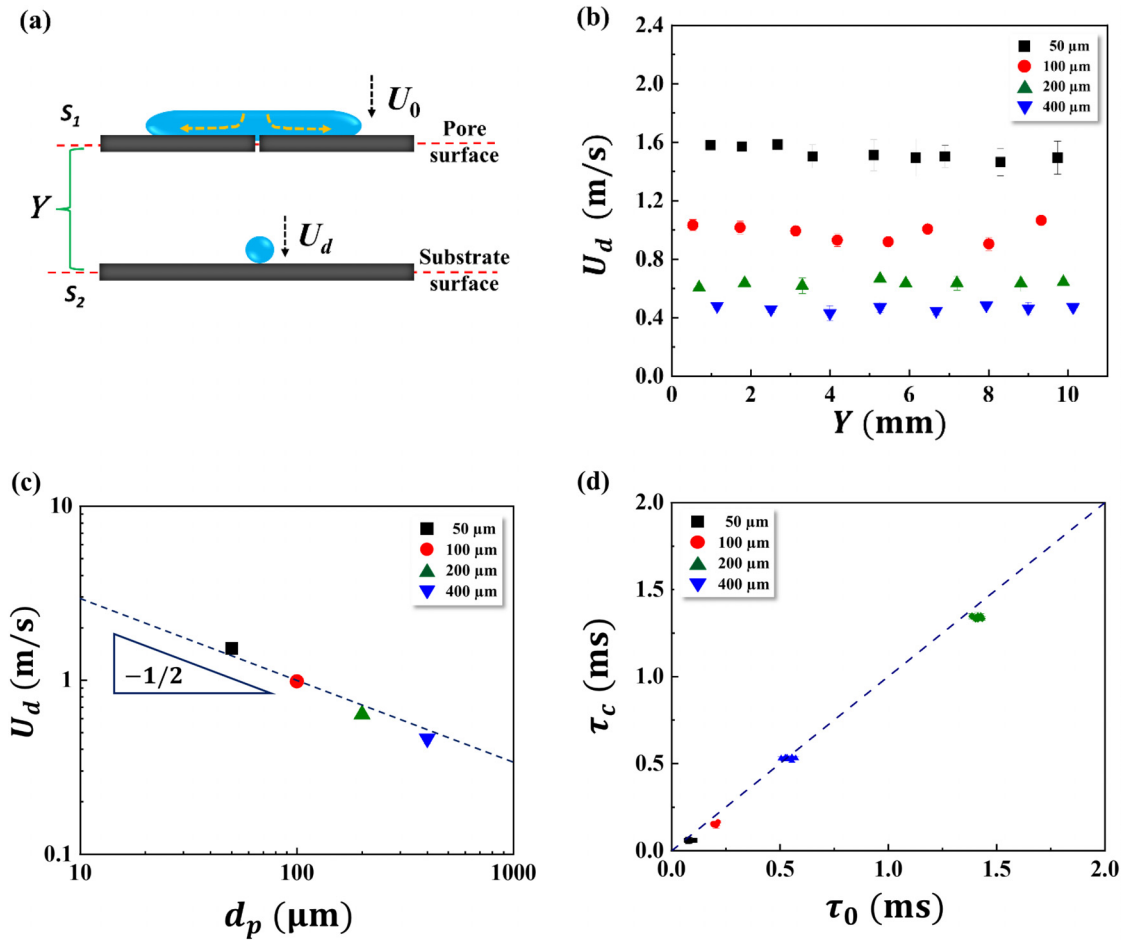
FIG. 5. (a) Schematic of droplet impact of the generated microdroplet on substrate surface. (b) Deposition velocity variation of the generated microdroplet as a function of spacing between the micropore surface S_1 and the substrate surface S_2. (c) Deposition velocity U_d as a function of the micropore diameter. (d) The measured contact time τ_c as a function of Rayleigh time τ_0; the dashed line represents $\tau_c = \tau_0$.

with the previous work, which reported the independence of microdroplet diameter on viscosity change.[8]

C. Dynamics of the generated microdroplet

After the microdroplet is generated, the microdroplet velocity can be important for certain applications such as microdroplet printing. Here, we varied the spacing Y between two surfaces S_1 and S_2 and studied how the impact velocity of the microdroplet on surface S_2 varies with Y [Fig. 5(a)]. In this experiment, the gap was increased up to 10.13 mm, and it was found that the impact velocity of the microdroplet remains constant [Fig. 5(b)] despite the change of Y.

Here, the averaged impact velocity was defined as the deposition velocity U_d, and the deposition velocity of the generated microdroplets was measured to be 0.47, 0.63, 0.98, and 1.50 mm/s for 400, 200, 100, and 50 μm micropores, respectively. Figure 5(c) shows the variation of deposition velocity with pore size. On a log–log scale, the deposition velocity decreases with pore diameter, d_p, such that $U_d \sim 1/\sqrt{d_p}$, following the same dependence on d_p as the critical impact velocity for liquid penetration.

Moreover, microdroplet generation allows experimental measurement of the contact time of a bouncing microdroplet. The measured contact time τ_c is shown in Fig. 5(d), where τ_c increases with increase in the microdroplet diameter d_m. The results show that the contact time is also determined by the Rayleigh timescale, $\tau_0 = \pi/\sqrt{2}\sqrt{\rho\,(d_m/2)^3\gamma^{-1}}$, which has been shown to be valid with millimeter-size drops.[39] Here, the measured contact time τ_c is plotted as a function of the Rayleigh contact time τ_0 as shown in Fig. 5(d), showing good agreement with the theoretical prediction.

D. Application examples

The generation of microdroplets in the range of a few hundreds of micrometers can be utilized for several practical applications. Here, we suggest two potential applications of microdroplets.

Figure 6(a) shows the demonstration of microdroplet ink printing on a paper. Here, a paper was used as a secondary substrate below a micropore, and an ink drop was impacted on a single micropore with 100 μm diameter. To print multiple microdroplets, a paper was moved
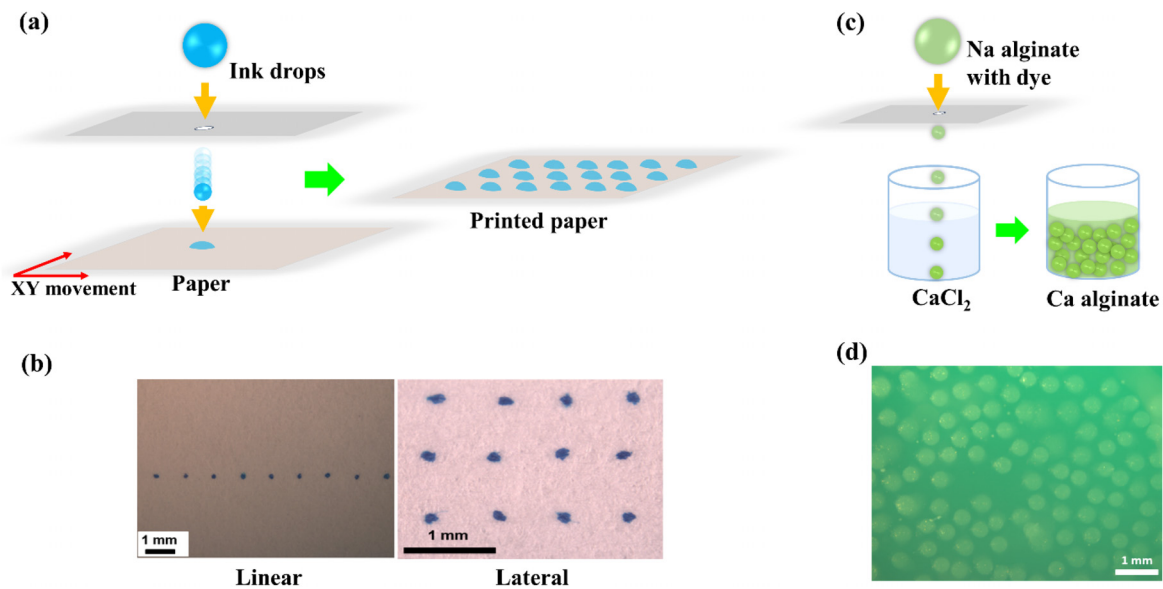
FIG. 6. (a) Schematic illustrating pattern printing using microdroplets of ink. (b) Results showing linear and lattice patterns achieved with a pore diameter of 100 μm at a targeted distance of 1000 μm (size: 180 μm). (c) Schematic depicting calcium alginate microbead fabrication through the drop impact method using a 400 μm pore. (d) Microbead fabrication using sodium alginate in a calcium chloride solution (bead size: 420–484 μm).

in the linear and lateral direction with an automatically controlled XY-linear stage (VIGOTEC, VG-X4). It would be desirable to minimize the gap between the paper and the pore to avoid printing errors. At the same time, the gap needs to be larger than the liquid jet length required for a single microdroplet generation. After taking these two criteria into account, the gap was set to be 600 μm during this experiment. The printing distance between two subsequent microdroplets was set as 1 mm and a uniform lattice pattern could be created with an average pattern diameter of 180 μm [Fig. 6(b)], demonstrating successful pattern printing using the present technique.

As another potential application, the microbead formation is shown in Fig. 6(c). It has been shown that a solution of sodium alginate (Sigma-Aldrich) becomes gelated (i.e., calcium alginate) upon interaction with calcium chloride (Daejung Co. Ltd.), and these gelated hydrogel microbeads can be utilized for the delivery of drugs or proteins.[40,41] Figure 6(c) displays the schematic of our approach to generate calcium alginate microbeads by impinging a sodium alginate drop onto a micropore with 400 μm diameter. Here, sodium alginate was mixed with a dye (fluorescein sodium salt, 46960, Sigma-Aldrich) for visualization. Beneath a micropore, a solution of calcium chloride was placed to collect and solidify the generated microdroplet of solidum alginate. Upon contact with the calcium chloride solution, a sodium alginate microdroplet was cured and calcium alginate microbead was formed with its diameter ranging between 420 and 484 μm [Fig. 6(d)]. It is found that this microbead diameter is smaller than the expected microdroplet diameter, probably due to the shrinkage of microbead after curing.

The foundational studies discussed previously have established the critical roles of viscosity and pore size in practical applications. For instance, our examination of ink with a viscosity of 4.9 cP and sodium alginate with a viscosity of 20 cP has reinforced our primary findings concerning the impact velocity necessary for generating a single microdroplet. Moreover, our experimental results have confirmed the proportionality between the sizes of the produced ink droplets and microbeads to the diameter of the micropores. This finding affirms the strength of our theoretical framework and its ability to accurately predict the behavior of microdroplets across various applications.

IV. CONCLUSIONS

In conclusion, our extensive experiments have confirmed the practicality of generating single microdroplets through drop impact on superhydrophobic micropores, with the superhydrophobicity ensuring complete pore dewetting post-generation. This research has successfully established the parameters for single microdroplet formation, relating micropore diameter and liquid viscosity. We determined the necessity for an optimal impact velocity—high enough to counteract the capillary forces within the micropore, stretching the liquid into a jet of adequate length, yet not so high as to create multiple microdroplets. Additionally, we examined the subsequent dynamics of microdroplets, including their deposition velocity onto substrates and the duration of contact with superhydrophobic surfaces. Ultimately, our work showcases two practical applications: precision pattern printing and microbead fabrication. We are confident that this study has shed light on the intricate mechanisms of microdroplet generation within micropores and will open up new avenues for microdroplet-based printing techniques in various applications.

SUPPLEMENTARY MATERIAL

See the supplementary material for additional data (supplementary Figs. S1, S2, and Table S1).

AUTHOR DECLARATIONS

Conflict of Interest

The authors have no conflicts to disclose.

Author Contributions

Mohammad Shibli Reza: Data curation (equal); Formal analysis (equal); Investigation (equal); Methodology (equal); Visualization (equal); Writing – original draft (equal). **Young-Su Ko:** Data curation (equal); Formal analysis (equal); Investigation (equal); Methodology (equal). **Byeong Eun Jeon:** Data curation (equal); Formal analysis (equal); Investigation (equal); Methodology (equal); Visualization (equal). **Prosenjit Sen:** Conceptualization (equal); Project administration (equal); Supervision (equal); Writing – review & editing (equal). **Choongyeop Lee:** Conceptualization (equal); Funding acquisition (equal); Project administration (equal); Supervision (equal); Validation (equal); Writing – review & editing (equal).

DATA AVAILABILITY

The data that support this study are available within the article and supplementary material.

REFERENCES

[1] H. Gudapati, M. Dey, and I. Ozbolat, "A comprehensive review on droplet-based bioprinting: Past, present and future," Biomaterials **102**, 20–42 (2016).

[2] M. Balzan, A. Abdollahi, F. S. Wells, and G. R. Willmott, "Drop impact of non-Newtonian dairy-based solutions," Colloids Surf., A **625**, 126895 (2021).

[3] C. Park, J. Seol, A. Aldalbahi, M. Rahaman, A. L. Yarin, and S. S. Yoon, "Drop impact phenomena and spray cooling on hot nanotextured surfaces of various architectures and dynamic wettability," Phys. Fluids **35**(2), 027126 (2023).

[4] S. Khandekar, G. Sahu, K. Muralidhar, E. Y. Gatapova, O. A. Kabov, R. Hu, X. Luo, and L. Zhao, "Cooling of high-power LEDs by liquid sprays: Challenges and prospects," Appl. Therm. Eng. **184**, 115640 (2021).

[5] U. C. Yi and C. J. Kim, "Soft printing of droplets pre-metered by electrowetting," Sens. Actuators, A **114**(2–3), 347–354 (2004).

[6] X. Chen, A. P. O'Mahony, and T. J. Barber, "Effect of 3D-bioprinted droplet impact dynamics on a pre-printed soft hydrogel matrix," Exp. Fluids **64**(3), 60 (2023).

[7] M. Abouelsoud, A. Kherbeche, and M. J. Thoraval, "Drop impact on a mesh—Viscosity effect," J Colloid Interface Sci. **648**, 37–45 (2023).

[8] C. D. Modak, A. Kumar, A. Tripathy, and P. Sen, "Drop impact printing," Nat. Commun. **11**(1), 4327 (2020).

[9] S. Ryu, P. Sen, Y. Nam, and C. Lee, "Water penetration through a superhydrophobic mesh during a drop impact," Phys. Rev. Lett. **118**(1), 014501 (2017).

[10] B. P. Croom, A. Abbott, J. W. Kemp, L. Rueschhoff, L. Smieska, A. Woll, S. Stoupin, and H. Koerner, "Mechanics of nozzle clogging during direct ink writing of fiber-reinforced composites," Addit. Manuf. **37**, 101701 (2021).

[11] J. Li, F. Rossignol, and J. Macdonald, "Inkjet printing for biosensor fabrication: Combining chemistry and technology for advanced manufacturing," Lab Chip **15**(12), 2538–2558 (2015).

[12] B. S. Yilbas, G. Hassan, A. Al-Sharafi, H. Ali, N. Al-Aqeeli, and A. Al-Sarkhi, "Water droplet dynamics on a hydrophobic surface in relation to the self-cleaning of environmental dust," Sci. Rep. **8**(1), 2984 (2018).

[13] G. Hassan, B. S. Yilbas, A. Al-Sharafi, and H. Al-Qahtani, "Self-cleaning of a hydrophobic surface by a rolling water droplet," Sci. Rep. **9**(1), 5744 (2019).

[14] X. Wang, D. L. Sun, X. D. Wang, and W. M. Yan, "Dynamics of droplets impacting hydrophilic surfaces decorated with a hydrophobic strip," Int. J. Heat Mass Transfer **135**, 235–246 (2019).

[15] C. Antonini, A. Amirfazli, and M. Marengo, "Drop impact and wettability: From hydrophilic to superhydrophobic surfaces," Phys. Fluids **24**(10), 102104 (2012).

[16] M. Miwa, A. Nakajima, A. Fujishima, K. Hashimoto, and T. Watanabe, "Effects of the surface roughness on sliding angles of water droplets on superhydrophobic surfaces," Langmuir **16**(13), 5754–5760 (2000).

[17] A. B. D. Cassie and S. Baxter, "Wettability of porous surfaces," Trans. Faraday Soc. **40**, 546–551 (1944).

[18] C. Lee, Y. Nam, H. Lastakowski, J. I. Hur, S. Shin, A. L. Biance, C. Pirat, C. J. Kim, and C. Ybert, "Two types of Cassie-to-Wenzel wetting transitions on superhydrophobic surfaces during drop impact," Soft Matter **11**(23), 4592–4599 (2015).

[19] T. Darmanin and F. Guittard, "Superhydrophobic and superoleophobic properties in nature," Mater. Today **18**(5), 273–285 (2015).

[20] S. Ge-Zhang, T. Cai, H. Yang, Y. Ding, and M. Song, "Biology and nature: Bionic superhydrophobic surface and principle," Front. Bioeng. Biotechnol. **10**, 1033514 (2022).

[21] Z. Wang, C. Lopez, A. Hirsa, and N. Koratkar, "Impact dynamics and rebound of water droplets on superhydrophobic carbon nanotube arrays," Appl. Phys. Lett. **91**(2), 023105 (2007).

[22] X. Li, X. Ma, and Z. Lan, "Dynamic behavior of the water droplet impact on a textured hydrophobic/superhydrophobic surface: The effect of the remaining liquid film arising on the pillars' tops on the contact time," Langmuir **26**(7), 4831–4838 (2010).

[23] J. Lomga, P. Varshney, D. Nanda, M. Satapathy, S. S. Mohapatra, and A. Kumar, "Fabrication of durable and regenerable superhydrophobic coatings with excellent self-cleaning and anti-fogging properties for aluminium surfaces," J. Alloys Compd. **702**, 161–170 (2017).

[24] P. Varshney, D. Nanda, M. Satapathy, S. S. Mohapatra, and A. Kumar, "A facile modification of steel mesh for oil-water separation," New J. Chem. **41**(15), 7463–7471 (2017).

[25] D. Nanda, A. Sahoo, A. Kumar, and B. Bhushan, "Facile approach to develop durable and reusable superhydrophobic/superoleophilic coatings for steel mesh surfaces," J. Colloid Interface Sci. **535**, 50–57 (2019).

[26] A. Kumar and B. Gogoi, "Development of durable self-cleaning superhydrophobic coatings for aluminium surfaces via chemical etching method," Tribol. Int. **122**, 114–118 (2018).

[27] Y. Liu, G. Whyman, E. Bormashenko, C. Hao, and Z. Wang, "Controlling drop bouncing using surfaces with gradient features," Appl. Phys. Lett. **107**(5), 051604 (2015).

[28] P. B. Weisensee, J. Tian, N. Miljkovic, and W. P. King, "Water droplet impact on elastic superhydrophobic surfaces," Sci. Rep. **6**, 30328 (2016).

[29] É. Lorenceau and D. Quéré, "Drops impacting a sieve," J. Colloid Interface Sci. **263**(1), 244–249 (2003).

[30] C. Boscariol, S. Chandra, D. Sarker, C. Crua, and M. Marengo, "Drop impact onto attached metallic meshes: Liquid penetration and spreading," Exp. Fluids **59**(12), 189 (2018).

[31] J. Eggers, M. A. Fontelos, C. Josserand, and S. Zaleski, "Drop dynamics after impact on a solid wall: Theory and simulations," Phys. Fluids **22**(6), 062101 (2010).

[32] L. Sun, S. Lin, B. Pang, Y. Wang, E. Li, X. Zu, K. Zhang, X. Xiang, and L. Chen, "Water sprays formed by impinging millimeter-sized droplets on superhydrophobic meshes," Phys. Fluids **33**(9), 092111 (2021).

[33] D. Soto, H. L. Girard, A. Le Helloco, T. Binder, D. Quéré, and K. K. Varanasi, "Droplet fragmentation using a mesh," Phys. Rev. Fluids **3**(8), 083602 (2018).

[34] C. Bae, S. Oh, J. Han, Y. Nam, and C. Lee, "Water penetration dynamics through a Janus mesh during drop impact," Soft Matter **16**(26), 6072–6081 (2020).

[35] M. J. Su, Y. Luo, G. W. Chu, Y. Cai, Y. Le, L. L. Zhang, and J. F. Chen, "Dispersion behaviors of droplet impacting on wire mesh and process intensification by surface micro/nano-structure," Chem. Eng. Sci. **219**, 115593 (2020).

[36] G. Wang, J. Gao, and K. H. Luo, "Droplet impacting a superhydrophobic mesh array: Effect of liquid properties," Phys. Rev. Fluids **5**(12), 123605 (2020).

[37] M. N. E. Alam and H. Tan, "Droplet impact on a microhole through a partially wetting surface," Phys. Fluids **35**(10), 102011 (2023).

[38] Y. Nam and Y. S. Ju, "A comparative study of the morphology and wetting characteristics of micro/nanostructured Cu surfaces for phase change heat transfer applications," J. Adhes. Sci. Technol. **27**(20), 2163–2176 (2013).

[39] D. Richard, C. Clanet, and D. Quéré, "Contact time of a bouncing drop," Nature **417**(6891), 811–811 (2002).

[40] K. Y. Lee and D. J. Mooney, "Alginate: Properties and biomedical applications," Prog. Polym. Sci. **37**(1), 106–126 (2012).

[41] Y. Cao, H. Cong, B. Yu, and Y. Shen, "A review on the synthesis and development of alginate hydrogels for wound therapy," J. Mater. Chem. B **11**(13), 2801–2829 (2023).